

# Evaluating the Impact of Inhibitory rTMS on Source-Localized BCI Training for Motor Imagery

Tony Chae\*

*Department of Electrical and Computer Engineering  
The University of Texas at Austin  
Austin, USA  
tsc2262@utexas.edu*

Everett Fletcher\*

*Department of Electrical and Computer Engineering  
The University of Texas at Austin  
Austin, USA  
emf2676@utexas.edu*

Haoran Niu\*

*Department of Electrical and Computer Engineering  
The University of Texas at Austin  
Austin, USA  
haoranniu@utexas.edu*

Yilin Zhou\*

*Department of Electrical and Computer Engineering  
The University of Texas at Austin  
Austin, USA  
maeby\_zhou@utexas.edu*

**Abstract**—Brain–computer interfaces (BCIs) leveraging motor imagery (MI) offer non-invasive control over external devices and hold promise for stroke rehabilitation through neuroplasticity. However, their training efficiency varies widely across users and is influenced by neural signal clarity. Prior work has explored improving signal quality via source localization, yet little is known about how neuromodulation—such as repetitive transcranial magnetic stimulation (rTMS)—interacts with source level BCI performance. Here we investigate the effect of low-frequency (1 Hz) rTMS on the cortical source dynamics underlying MI-based BCI control. Using a novel pipeline that combines motor hotspot identification via TMS, source projection from 38 sensorimotor EEG channels, and Riemannian decoding over localized motor parcels, we assess how inhibitory rTMS modulates feature separability. We show that although sensor-space Fisher discriminability increases with MI training and decreases post rTMS consistent with known cortical inhibition effects source-space features do not follow this pattern. Instead, classification accuracy remains at zero across two participants, and source discriminability does not improve, suggesting a mismatch between target engagement and feedback. These findings suggest that predefined source parcels may fail to capture actual user strategies during BCI learning, and that neuromodulatory effects are not uniformly reflected across measurement levels. Our results highlight the importance of verifying source-level engagement before using it for feedback, and inform future designs of adaptive BCI systems that align decoding targets with real-time neural dynamics.

**Index Terms**—rTMS, BCI, brain-computer interaction

## I. INTRODUCTION AND HYPOTHESIS

Brain–computer interfaces (BCIs) that translate motor-imagery (MI) into device or therapeutic stimulation control have emerged as promising tools for motor rehabilitation. They have the potential to induce neural plasticity by providing neurofeedback, helping patients re-engage motor networks following cortical insult. In post-stroke therapy, multiple reviews have shown that BCI-driven neurofeedback training may improve motor function of the upper extremities [1]. However,

performance with BCIs can be highly variable and have a steep learning curve. Sustained training is required for users to learn to control the BCI reliably, so facilitating this learning process and ensuring its neural specificity are critical for effective rehabilitation.

Transcranial magnetic stimulation (TMS) is a non-invasive neural treatment that uses a changing magnetic field to induce current in a specific area of the human brain. rTMS stands for repetitive transcranial magnetic stimulation, and is widely used to treat depression, headache, etc. [2] [3].

### A. Problem Statement

Adaptive training in the electrode space of motor-imager BCIs can improve decoding accuracy but may also induce maladaptive plasticity that undermines clinical outcomes. To avoid this, we propose shifting neuromodulation from the scalp to the cortical source level, leveraging individualized source localization to guide rTMS interventions. Given that low-frequency rTMS ( $\leq 1$  Hz) is known to inhibit cortical excitability, our central question is whether such inhibitory modulation will impair MI-BCI training accuracy? If so, to what extent? By applying source-informed low-frequency rTMS to the patient’s specifically localized motor generator regions and quantifying resultant changes in BCI performance, we aim to demonstrate any negative impact of inhibitory rTMS on motor-imagery decoding. Confirming a detrimental effect would help refine future studies by narrowing the rTMS frequency range most appropriate for enhancing, rather than hindering, MI-BCI training.

### B. Hypothesis

In this report, we hypothesize that low-frequency rTMS disrupts longitudinal MI-BCI based training by transiently inhibiting the motor hand area of the primary motor cortex. Utilizing source localization to isolate this motor region, we trained MI-BCI decoders on source-projected signals and

\*The four authors contributed equally to this work.

evaluated their efficacy in online sessions. We expected to observe decreased BCI classification performance following the low-frequency rTMS stimulation as well as decreased discriminability (quantified by Fisher scoring) in our feature set.

## II. BACKGROUND AND RELATED WORK

### A. Source Localization in BCI

Traditional EEG-based BCIs operate based on signals from scalp electrodes (sensor space) to detect user intent. These signals, however, mix contributions from both cortical and non-cortical sources due to electrical field propagation. Source localization algorithms address this limitation by projecting scalp measurements onto a map of the cortical surface, estimating region-specific brain activity. In sensorimotor-rhythm based BCIs, source localization can enhance user control by isolating activity from the primary motor cortex or other task-relevant areas while also attenuating activity from irrelevant sources. By constraining features to relevant motor areas, source-localized BCIs can reduce extraneous noise and potentially improve performance. In fact, a 2015 study showed that source-BCIs could yield a classification accuracy increase of up to 18.6% for individual task classification, and an increase of 12.7% for overall classification [4]. This demonstrates the promise of source localization to boost BCI accuracy by enhancing the signal-to-noise ratio. Additionally, users can imagine movements that directly map onto the intended action, like imagining hand flexion to control the flexion of a prosthetic hand rather than using an abstract strategy. Overall, source localization offers improved anatomical specificity and intuitive control, which are valuable for both performance and for steering neural plasticity in rehabilitation.

A further advantage is that source-originated features may help prevent maladaptive learning. In BCIs, if a user discovers that they may achieve control through inadvertent classification strategies such as counting or visualization, they might begin to reinforce these non-optimal patterns. These strategies can therefore undermine the rehabilitation goal, which is to induce plasticity in the cortical task area by reactivating relevant pathways. By focusing on cortical source activity, especially in target areas, the BCI can minimize input from irrelevant signals. Prior work in neurofeedback has emphasized matching the feedback signal to the specific brain region and frequency band of interest to drive plastic changes [5]. Source-localized BCIs align with this principle by providing feedback from, say, the lesioned motor cortex in stroke patients, which could strengthen use-dependent plasticity in that area.

### B. rTMS Effects on Cortical Excitability

Repetitive TMS can induce lasting changes in cortical excitability and has been explored as a means to modulate brain plasticity. The general findings suggest that low-frequency rTMS (around 1 Hz) inhibits cortical excitability, while higher frequency stimulation ( $\geq 5$  Hz) increases excitability [6]. These frequency-dependent effects provide a tool to either downregulate or upregulate specific cortical

areas. In rehabilitation, 1 Hz rTMS has been used to inhibit contralateral (healthy hemisphere) M1 to reduce its inhibitory grip on the stroke-affected hemisphere, aiming to rebalance interhemispheric interactions [7]. High-frequency rTMS has been applied to the lesioned M1 to promote greater excitability and facilitate motor relearning [8]. This suggests rTMS can acutely boost BCI-relevant signals. On the flip side, inhibitory rTMS might degrade those signals: a hypothesis directly tested in our study by delivering 1 Hz rTMS to the motor hotspot during an MI-BCI paradigm.

## III. EXPERIMENTAL SETUP AND METHODOLOGIES

### A. Experimental Protocol

The objective of this study is to investigate the effects of TMS on MI control in a BCI system. Two healthy volunteers from our group were selected for this study. Both participants have no neurological disorders and are capable of understanding and executing MI tasks. Throughout the experiment, electroencephalography (EEG) signals are continuously recorded, and real-time feedback is provided based on cortical source activation.

The study needs two days to complete. Day one consists of two sessions. In the first session, referred to as the BCI Calibration Session or the offline session, participants perform dominant-hand MI tasks, compared with a resting condition. The data from this session is used to construct the user-specific classifier. The following session is the online BCI session (which is composed of four runs), during which subjects continue to perform MI tasks while receiving real-time visual feedback on cortical source activation as measured by the classifier output.

Day two includes three sessions. The initial session is an offline session during which EEG data are recorded without feedback. This session is aimed at refining the parameters used for cortical source estimation. Next, an online BCI session (which includes three runs) is conducted analogous to those on Day 1 to acquire pre-rTMS performance data. Subsequently, rTMS is applied by first identifying the motor hotspot using a neuronavigation system, and then administering rTMS stimulation to modulate activity in the targeted motor cortex region. Finally, a post-TMS online BCI session (which also has three runs) is performed to assess the effects of rTMS on MI performance.

An overview of the experiment protocol is shown as Fig 1.

### B. Model Construction

To construct the subject-specific inverse model for source-space BCI training, we followed a three-stage pipeline: (1) Motor hotspot identification via single-pulse TMS to define the motor target area; (2) BCI input training using source-level data reconstructed from sensorimotor EEG channels; and (3) BCI feedback delivery, which was based exclusively on a subset of sources localized around the individualized motor region. EEG data were recorded from a 64-channel full-head montage, from which a subset of 38 channels covering the sensorimotor cortex was selected: F7, F5, F3, F1, Fz, FC5,

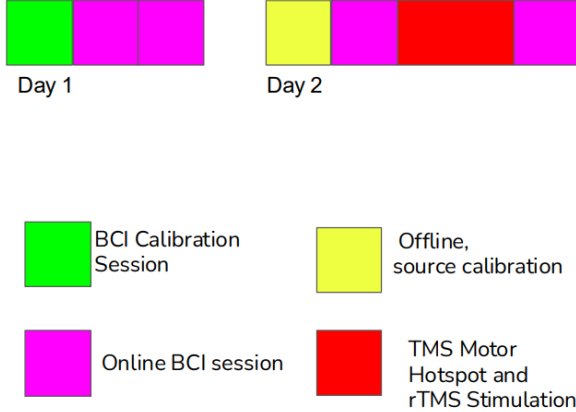


Fig. 1. The Experiment Protocol Overview.

FC3, FC1, FCz, C5, C3, C1, Cz, CP5, CP3, CP1, P7, P5, P3, P1, Pz, F8, F6, F4, F2, FC6, FC4, FC2, C6, C4, C2, CP6, CP4, CP2, P8, P6, P4, and P2. Source localization was applied to this subset to construct a source space composed of 44 cortical parcels.

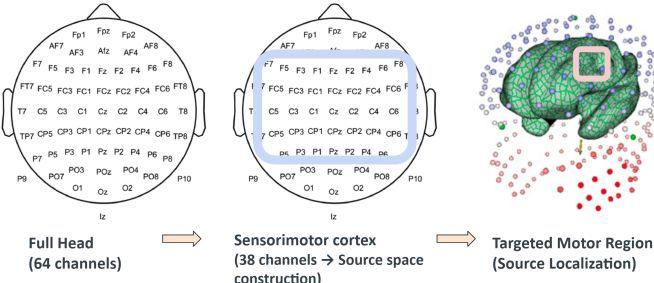


Fig. 2. Model Construction Pipeline

Among these, 4 parcels located near the TMS-defined motor hotspot were used to compute the BCI control signal. For decoding, we employed a Riemannian geometry-based decoder, in which the covariance matrix  $\mathbf{C}_i \in \mathbb{R}^{d \times d}$  of each trial  $i$  is treated as a point on the manifold of symmetric positive definite (SPD) matrices. Classification is then based on the geodesic distance between each trial's covariance matrix and class-mean covariance matrices. The Riemannian mean  $\bar{\mathbf{C}}$  for a class is computed as the matrix that minimizes the sum of squared affine-invariant distances (AIRM):

$$\bar{\mathbf{C}} = \arg \min_{\mathbf{C}} \sum_{i=1}^N \delta_R^2(\mathbf{C}, \mathbf{C}_i)$$

where  $\delta_R(\mathbf{C}_1, \mathbf{C}_2) = \|\log(\mathbf{C}_1^{-1/2} \mathbf{C}_2 \mathbf{C}_1^{-1/2})\|_F$  is the Affine-Invariant Riemannian Metric (AIRM) between two SPD matrices. This method allows for robust classification in source space by leveraging the intrinsic geometry of covariance matrices. Critically, BCI performance feedback was generated

solely from the 4-parcel subspace near the motor hotspot, ensuring that feedback reflected modulation of only the relevant cortical area targeted by the TMS. The model construction pipeline is shown in Fig. 2

### C. Data Preprocessing

As described in Section III-A, our study has both offline calibration sessions and online BCI sessions with visual feedback. In this report, we focus on the three online sessions (one online session on day one and two online sessions on day two) since our problem statement and hypothesis focus on the performance of MI-BCI training. We name the online session in day one as “session one”. Likewise, we call the two online sessions on day two “session two” and “session three” respectively.

After the two subjects finished the day one and day two sessions mentioned in section III-A, the training data were generated to the files in *.gdf* format, one *.gdf* file per run. The *.gdf* files contain header information about triggers and channels as well as EEG signals.

To process the data, below are the steps we take:

- We extract the data of the three online sessions, which are 10 *.gdf* files in total.
- We read the *.gdf* files with Python *mne* library to get the EEG signals and use Matlab EEGLAB toolbox to extract the struct of header information.
- We re-construct the data structure as Figure 3.

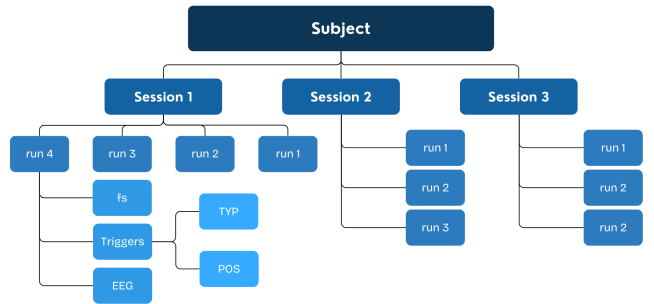


Fig. 3. Reconstructed Data Structure Using the Data from the *.gdf* Files.

### D. Feature Extraction

EEG-based BCI performance depends critically on selecting features that capture the relevant neural dynamics and pairing them with effective classifiers. In the sensor domain, we extract spectral power in the mu (8–13 Hz) and beta (13–30 Hz) bands because event-related desynchronization (ERD) in these rhythms reliably indexes motor imagery activity [9].

In our analysis, for each run of each session, we extract its feature of power spectral density. Power spectral density is estimated using Welch’s method (*pwelch*) over 4–30 Hz with 2 Hz resolution—balancing frequency precision with temporal stability in short windows.

In the source domain, we captured the activity of four cortical sources in the motor cortex. To capture the coordinated dynamics of these parcels, we represent each trial by the covariance matrix of their mu-band time series. Covariance inherently encodes both the power within each parcel and the pairwise interactions between parcels. This encoding reflects the functional connectivity patterns that underlie motor imagery [10]. From each covariance matrix, we extract the following descriptors:

- **MaxEig**: largest eigenvalue,  $\lambda_{\max}$ ;
- **EigRatio**: ratio of largest to smallest eigenvalue,  $\lambda_{\max}/\lambda_{\min}$ ;
- **FrobNorm**: Frobenius norm,  $\|C\|_F$ ;
- **LogDet**: log-determinant,  $\log \det(C)$ ;
- **Trace**: trace of the matrix,  $\text{tr}(C)$ .

These five features attempt to summarize the variance distribution and overall magnitude of inter-parcel coupling, providing a compact, low-dimensional representation.

#### E. MI-BCI Training Performance Metrics

To evaluate how well the two subjects perform during the BCI online sessions, we leverage two metrics: command delivery accuracy and timeout percentage. Denote  $\#Hits$  as the number of times that a subject delivers a BCI command correctly. Denote  $\#timeouts$  as the number of timeouts a subject experiences when trying to deliver a BCI command. Moreover,  $\#trials$  represents the number of trials per run.

For each run in each session per subject, the formula for calculating the BCI command delivery accuracy  $acc$  is:  $acc = \frac{\#Hits}{\#Hits + \#timeouts}$ . The timeout percentage  $p$  is:  $p = \frac{\#timeouts}{\#trials}$ .

Both subjects in our group do not have a good performance in MI-BCI training. The precision of the BCI command delivery for both is almost zero, and their timeout percentage is almost 100%. However, we still have promising findings despite the poor performance of the MI-BCI training, which we will explain in Section IV.

## IV. RESULT ANALYSIS AND VISUALIZATION

### A. Fisher Score Analysis

The Fisher score [11] is commonly used for feature selection. In this project, since we have two classes (rest and move), we calculate the fisher scores based on the PSD values extracted from the rest and the move classes respectively. Suppose the PSD values of the rest class for each trial of each run is  $p_1$ .  $p_2$  presents the PSD values of the move class for each trial of each run.

To quantify changes in feature discriminability across sessions, we conducted paired-sample  $t$ -tests on the mean channel Fisher scores. Tables I–IV summarize the per-subject results for all 64 channels (“Full-Head”) and for the subset over sensorimotor electrodes (“Sensorimotor Channels”). Table V reports group-level paired  $t$ -tests on the average Fisher score across subjects, and Table VI lists the top three channel–frequency features by session.

a) *Subject-Level Results*: For Subject 1 (Table I), Fisher scores rose markedly from Session 1 to Session 2 ( $\Delta = +0.0849$ ,  $d = 2.11$ ,  $p < 10^{-24}$ ), then declined after rTMS (Session 2→3:  $\Delta = -0.0382$ ,  $d = -1.20$ ,  $p < 10^{-13}$ ). The net change from Session 1→3 remained positive ( $\Delta = +0.0467$ ,  $d = 1.30$ ,  $p < 10^{-14}$ ). The sensorimotor subset (Table II) showed the same overall trend.

Subject 2 (Tables III, IV) exhibited a similar pattern: significant gains with training followed by decreases post-rTMS.

b) *Group-Level Analysis*: Combining both subjects, Table V confirms these effects at the group scale: Fisher scores increased from Session 1→2 ( $t(127) = 17.05$ ,  $d = 1.51$ ,  $p \approx 10^{-34}$ ) and then decreased from Session 2→3 ( $t(127) = -15.45$ ,  $d = -1.37$ ,  $p \approx 10^{-31}$ ) across both full-head and sensorimotor channels.

c) *Boxplot Distributions*: Figures 4–9 show the session-wise distributions of mean Fisher scores for each condition:

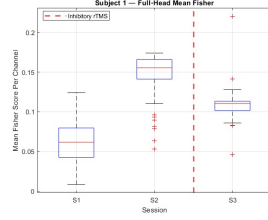


Fig. 4. Subject 1 — Full-Head Fisher Score by Session

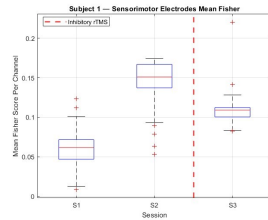


Fig. 5. Subject 1 — Sensorimotor Fisher Score by Session

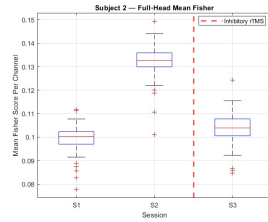


Fig. 6. Subject 2 — Full-Head Fisher Score by Session

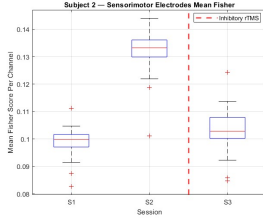


Fig. 7. Subject 2 — Sensorimotor Fisher Score by Session

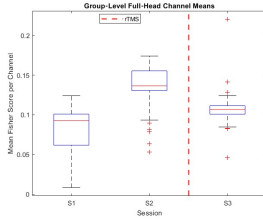


Fig. 8. Group — Full-Head Fisher Score by Session

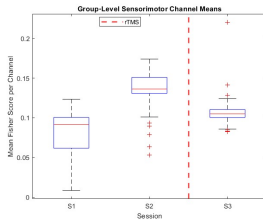


Fig. 9. Group — Sensorimotor Fisher Score by Session

In each plot, the mean Fisher score increases from Session 1 to Session 2, then decreases in Session 3, matching the statistical results. This pattern is consistent across all subplots—demonstrating that both full-head and sensorimotor feature sets show the expected learning-gain then rTMS-induced drop in discriminability.

*d) Feature-Level Insights:* Table VI highlights the top three channel-frequency features per session. These features peak in discriminability after training (Session 2) and decline following stimulation (Session 3).

*e) Interpretation:* Across statistical tests and distributional analyses, we observe a robust increase in Fisher scores with training, followed by a reproducible decrease after low-frequency rTMS. This confirms our hypothesis that inhibitory rTMS transiently impairs the neural separability underlying MI-BCI control. The effect is evident in both broad (full-head) and focused (sensorimotor) feature sets, underscoring its generalizability.

#### B. Topoplot Analysis

For each subject, we calculate the fisher scores for all 64 channels. The results are shown as Fig. 10 and 11. In the topoplots, a brighter color indicates a higher fisher score. Moreover, a higher fisher score implies a better discriminability between the rest and the move class. For both subjects, the

TABLE I  
SUBJECT 1 — FULL-HEAD

Contrast	$\Delta$	$d$	$p$
$S1 \rightarrow S2$	+0.0849	+2.11	5.01e-25
$S2 \rightarrow S3$	-0.0382	-1.20	5.86e-14
$S1 \rightarrow S3$	+0.0467	+1.30	2.83e-15

TABLE II  
SUBJECT 1 — SENSORIMOTOR CHANNELS

Contrast	$\Delta$	$d$	$p$
$S1 \rightarrow S2$	+0.0837	+2.00	1.07e-14
$S2 \rightarrow S3$	-0.0351	-0.95	1.07e-06
$S1 \rightarrow S3$	+0.0486	+1.34	6.29e-10

TABLE III  
SUBJECT 2 — FULL-HEAD

Contrast	$\Delta$	$d$	$p$
$S1 \rightarrow S2$	+0.0330	+3.36	3.11e-36
$S2 \rightarrow S3$	-0.0287	-2.33	2.67e-27
$S1 \rightarrow S3$	+0.0043	+0.49	2.45e-04

TABLE IV  
SUBJECT 2 — SENSORIMOTOR CHANNELS

Contrast	$\Delta$	$d$	$p$
$S1 \rightarrow S2$	+0.0331	+3.92	2.91e-24
$S2 \rightarrow S3$	-0.0294	-2.19	7.39e-16
$S1 \rightarrow S3$	+0.0037	+0.41	1.51e-02

TABLE V  
GROUP-LEVEL PAIRED  $t$ -TESTS ON MEAN FISHER CHANNEL SCORES

All-Channels			Sensorimotor				
Contrast	$t(df)$	$d$	$p$	Contrast	$t(df)$	$d$	$p$
$S1 \rightarrow S2$	$t(127) = 17.05$	+1.51	1.25e-34	$S1 \rightarrow S2$	$t(75) = 12.95$	+1.49	8.17e-21
$S2 \rightarrow S3$	$t(127) = -15.45$	-1.37	5.91e-31	$S2 \rightarrow S3$	$t(75) = -10.08$	-1.16	1.35e-15
$S1 \rightarrow S3$	$t(127) = 8.57$	+0.76	3.04e-14	$S1 \rightarrow S3$	$t(75) = 6.59$	+0.76	5.47e-09

TABLE VI  
TOP THREE DISCRIMINATIVE FEATURES BY SESSION

Feat	Band	Chan	S1	S2	S3
F#1	16 Hz	10	0.1583	0.3587	0.1575
F#2	24 Hz	20	0.0329	0.3454	0.2934
F#3	24 Hz	58	0.2404	0.3447	0.3592

topoplot of session two has the brightest area, which means subjects' performance improves from session one to session two and drops from session two to session three. The topoplot results are consistent with our hypothesis of low-frequency rTMS disrupts longitudinal MI-BCI training.

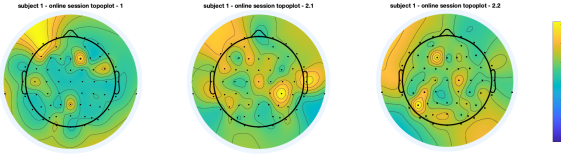


Fig. 10. Topoplots for Subject 1 on Session One, Two and Three.

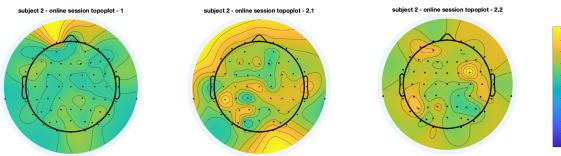


Fig. 11. Topoplots for Subject 2 on Session One, Two and Three.

### C. Grand Average Analysis

*a) EEG Analysis:* The grand average EEG analysis presented in Figure 12 demonstrates variations in peak and trough amplitudes between rest and task conditions across sessions; however, these differences are not readily discernible in the time-domain representation. To improve interpretability, we performed a power spectral density (PSD) analysis, which transforms the EEG data into the frequency domain, thereby enabling a more quantifiable evaluation of these differences.

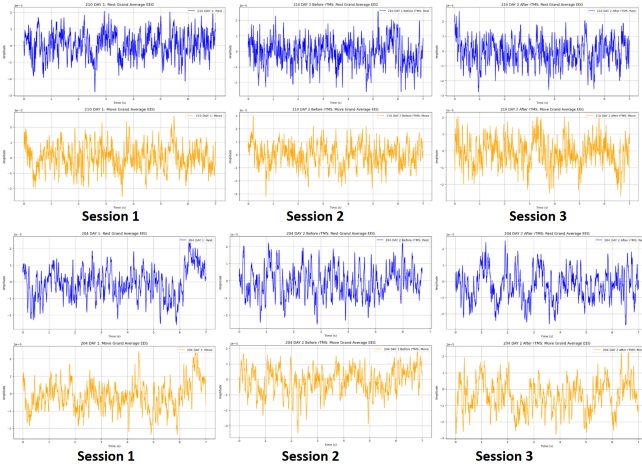


Fig. 12. Grand Average EEG Plot of Two Subjects Across Three Sessions

*b) PSD Analysis:* As shown in Figure 13, the PSD analysis reveals marked differences between the task and rest conditions within the 0–25 Hz frequency range. To further quantify these differences, we conducted an integral analysis by computing the area under the PSD curve over specified frequency bands. This approach facilitates a comprehensive

assessment of spectral power distribution and more clearly distinguishes neural activity disparities than conventional time-domain analysis.

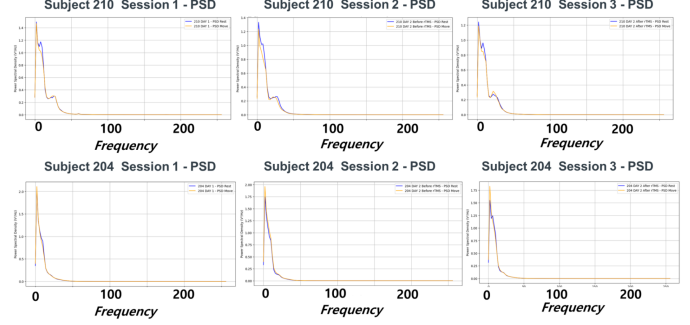


Fig. 13. Grand Average PSD Plot Across Three Sessions

*c) Integral Analysis:* Integral analysis quantifies the energy distribution of EEG signals within a defined frequency range by calculating the area under the PSD curve. This method is particularly effective for capturing cumulative power differences between task and rest conditions, as it aggregates the spectral contributions within key frequency bands.

Our integral analysis yields trends similar to those observed in our Fish Score analysis. In Session 1, the difference between task and rest conditions is minimal, whereas in Session 2, the difference peaks. Following the introduction of rTMS, the difference diminishes. Specifically, in the 0–50 Hz frequency range, the two conditions exhibit a pronounced disparity, while beyond 50 Hz the values converge and stabilize. These findings support our hypothesis that rTMS negatively impacts BCI performance by disrupting the neural dynamics that underlie task execution.

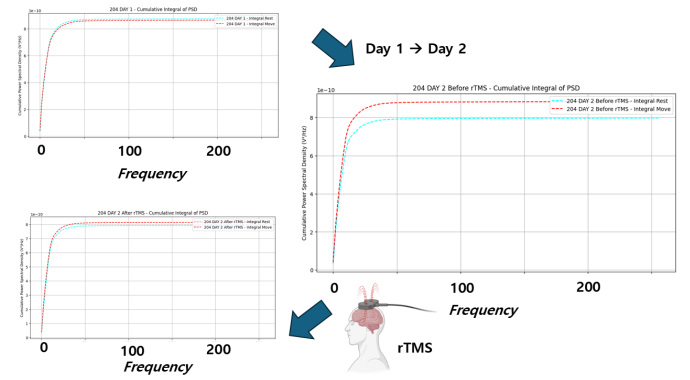


Fig. 14. Grand Average PSD Integral Plot of Subject 1 Across Three Sessions

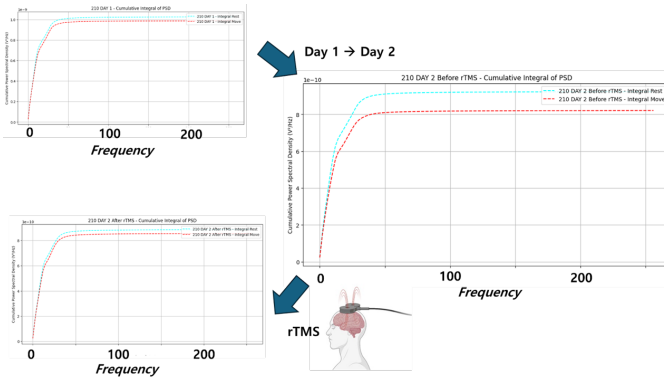


Fig. 15. Grand Average PSD Integral Plot of Subject 2 Across Three Sessions

#### D. Source Space Feature Analysis

Next, we examined the Fisher discriminability of our covariance-based source features across sessions. Figures 16–18 show the bar-plot of each feature’s Fisher score, and Figures 19–21 display boxplots of the mean Fisher score per trial, for Subject 1, Subject 2, and the Group.

*a) Lack of Expected Trend:* Contrary to our hypothesis, none of the three source-space plots exhibited the characteristic increase from Session 1 to 2 followed by a decrease in Session 3. Instead, feature-level scores either remained flat across all sessions or showed irregular fluctuations. The mean-score boxplots similarly revealed no consistent session-to-session change in median or interquartile range. This absence of the expected learning-gain and rTMS-induced drop suggests that, although participants did improve in sensor-space BCI control, those gains did not manifest robustly in the predefined source parcels.

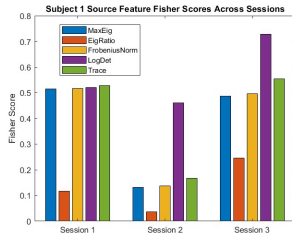


Fig. 16. Subject 1: Bar-plot of Fisher scores for each source feature across Sessions 1–3.

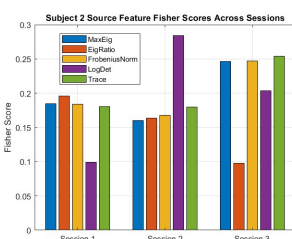


Fig. 17. Subject 2: Bar-plot of Fisher scores for each source feature across Sessions 1–3.

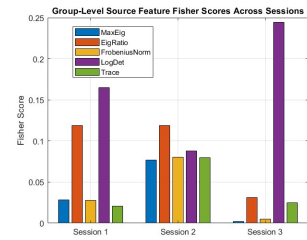


Fig. 18. Group: Bar-plot of Fisher scores for each source feature across Sessions 1–3.

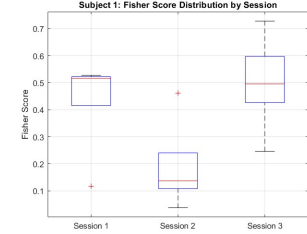


Fig. 19. Subject 1: Boxplot of mean source-feature Fisher scores per trial across sessions.

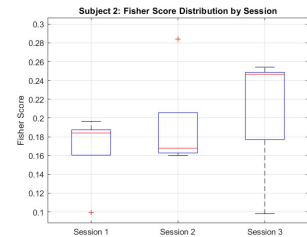


Fig. 20. Subject 2: Boxplot of mean source-feature Fisher scores per trial across sessions.

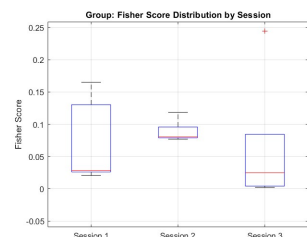


Fig. 21. Group: Boxplot of mean source-feature Fisher scores per trial across sessions.

*b) Consistent Null Effect Across Feature Sets:* All six plots consistently failed to show the hypothesized pattern. This null effect in source space—despite clear session-dependent changes in sensor-space features—indicates that participants did not reliably modulate the targeted cortical parcels during motor imagery, or that our inverse modeling smoothed away session-specific differences. Consequently, source-space discriminability remained largely invariant to both training and rTMS intervention.

c) *Implications:* The mismatch between sensor- and source-space results underscores the importance of verifying actual parcel engagement when using source-localized feedback. Without clear session-wise improvements in the intended sources, the BCI may have reinforced alternative cortical strategies, explaining the zero source-space classification accuracy and highlighting a key limitation of relying solely on predefined source targets.

## V. CONCLUSION AND DISCUSSION

In this study, both participants (Subjects 1 and 2) exhibited zero classification accuracy in the source-space BCI performance, which raises important limitations to consider. One potential reason is subject-specific anatomical and physiological factors that affected source targeting. Subject 204 had previously undergone ligament transplant surgery in the leg, and as a result, accurate identification of the motor hotspot for finger movement using single-pulse TMS was impeded, likely due to altered or masked motor cortical representations. Similarly, Subject 210 displayed extreme sensitivity in the ocular region, which complicated consistent stimulation and localization efforts.

Additionally, source localization itself introduces potential confounding factors. The inverse problem is highly sensitive to inter-individual differences in skull conductivity and head tissue geometry, which can introduce significant spatial noise and reduce signal precision. This could have adversely impacted the accuracy of source-space feature extraction and classification.

Interestingly, although source-space decoding failed, the sensor-space (electrode-level) Fisher discriminability scores followed our original hypothesis: an increasing trend across sessions 1 and 2 (pre-rTMS), followed by a decline after rTMS in session 3. This suggests that learning and adaptation did occur at the scalp-level (full head). However, when examining source-space features (e.g., covariance trace or maximum eigenvalue used in our Riemannian decoder), this trend was not observed. Instead, source-space discriminability either decreased during training or remained flat, suggesting that learning did not effectively engage the target source regions, even though it was these regions from which subjects received feedback.

This discrepancy can be explained by multiple neurophysiological mechanisms. First, the neural efficiency hypothesis suggests that task learning can reduce the variance in neural activation in task-relevant areas, leading to decreased discriminability despite improved performance. Second, maladaptive overfocusing may have occurred, where the patients engaged non-target (e.g., non-M1) areas during training, resulting in a suppression of activity in the intended motor regions. Third, volume conduction in scalp EEG may have masked the lack of true engagement in the motor parcel by capturing mixed signals from other regions, thus producing inflated Fisher scores at the sensor level.

Importantly, rTMS inhibition may have partially reversed maladaptive circuitry, as observed in some recovery of source

discriminability post-stimulation. Nevertheless, the consistent failure of the source-space decoder, despite clear learning effects in the electrode space, suggests that patients were not modulating the intended source parcel, and thus received feedback that did not align with their actual neural strategies. This misalignment likely contributed to the observed zero accuracy, highlighting a major limitation in relying solely on predefined source targets for BCI feedback without verifying actual subject engagement.

## VI. ACKNOWLEDGMENT

This research was conducted as part of the 374N/385J Neural Engineering course led by Professor José del R. Millán at The University of Texas at Austin. We would like to thank Akhil Surapaneni, Minsu Zhang, and Allan Frederick for their valuable assistance in data collection. We also gratefully acknowledge the support provided by the Cockrell School of Engineering at UT Austin.

## REFERENCES

- [1] Z. Bai, K. N. Fong, J. J. Zhang, J. Chan, and K. Ting, “Immediate and long-term effects of bci-based rehabilitation of the upper extremity after stroke: a systematic review and meta-analysis,” *Journal of neuroengineering and rehabilitation*, vol. 17, pp. 1–20, 2020.
- [2] J. Downar and Z. J. Daskalakis, “New targets for rtms in depression: a review of convergent evidence,” *Brain stimulation*, vol. 6, no. 3, pp. 231–240, 2013.
- [3] J. M. Stilling, O. Monchi, F. Amoozegar, and C. T. Debert, “Transcranial magnetic and direct current stimulation (tms/tcds) for the treatment of headache: A systematic review,” *Headache: The Journal of Head and Face Pain*, vol. 59, no. 3, pp. 339–357, 2019.
- [4] B. J. Edelman, B. Baxter, and B. He, “Eeg source imaging enhances the decoding of complex right-hand motor imagery tasks,” *IEEE Transactions on Biomedical Engineering*, vol. 63, no. 1, pp. 4–14, 2015.
- [5] J. Rogala, K. Jurewicz, K. Paluch, E. Kublik, R. Cetnarski, and A. Wróbel, “The do’s and don’ts of neurofeedback training: a review of the controlled studies using healthy adults,” *Frontiers in human neuroscience*, vol. 10, p. 301, 2016.
- [6] A. M. Speer, T. A. Kimbrell, E. M. Wassermann, J. D. Repella, M. W. Willis, P. Herscovitch, and R. M. Post, “Opposite effects of high and low frequency rtms on regional brain activity in depressed patients,” *Biological psychiatry*, vol. 48, no. 12, pp. 1133–1141, 2000.
- [7] N. N. Johnson, J. Carey, B. J. Edelman, A. Doud, A. Grande, K. Lakshminarayanan, and B. He, “Combined rtms and virtual reality brain-computer interface training for motor recovery after stroke,” *Journal of neural engineering*, vol. 15, no. 1, p. 016009, 2018.
- [8] T. Jia, L. Mo, C. Li, A. Liu, Z. Li, and L. Ji, “5 hz rtms improves motor-imagery based bci classification performance,” in *2021 43rd Annual International Conference of the IEEE Engineering in Medicine & Biology Society (EMBC)*. IEEE, 2021, pp. 6116–6120.
- [9] P. Herman, G. Prasad, T. M. McGinnity, and D. Coyle, “Comparative analysis of spectral approaches to feature extraction for eeg-based motor imagery classification,” *IEEE Transactions on Neural Systems and Rehabilitation Engineering*, vol. 16, no. 4, pp. 317–326, 2008.
- [10] M. Congedo, A. Barachant, and R. Bhatia, “Riemannian geometry for eeg-based brain-computer interfaces: a primer and a review,” *Brain-Computer Interfaces*, vol. 4, no. 3, pp. 155–174, 2017.
- [11] R. O. Duda, P. E. Hart, and D. G. Stork, “Chapter 8. pattern classification,” *A Wiley-Interscience Publication*, 2001.